UCRL-JC-130148
PREPRINT

# The Effects of Electron Spiraling on the Anisotropy and Polarization of Photon Emission from an Electron Beam Ion Trap

D. W. Savin, M. F. Gu, P. Beiersdorfer

This paper was prepared for submittal to the
Proceedings of the US - Japan Workshop on Plasma Polarization on Spectroscopy
Kyoto, Japan
January 26-28, 1998

March 5, 1998

Lawrence Livermore National Laboratory

This is a preprint of a paper intended for publication in a journal or proceedings. Since changes may be made before publication, this preprint is made available with the understanding that it will not be cited or reproduced without the permission of the author.

DISCLAIMER

This document was prepared as an account of work sponsored by an agency of the United States Government. Neither the United States Government nor the University of California nor any of their employees, makes any warranty, express or implied, or assumes any legal liability or responsibility for the accuracy, completeness, or usefulness of any information, apparatus, product, or process disclosed, or represents that its use would not infringe privately owned rights. Reference herein to any specific commercial product, process, or service by trade name, trademark, manufacturer, or otherwise, does not necessarily constitute or imply its endorsement, recommendation, or favoring by the United States Government or the University of California. The views and opinions of authors expressed herein do not necessarily state or reflect those of the United States Government or the University of California, and shall not be used for advertising or product endorsement purposes.

# The effects of electron spiraling on the anisotropy and polarization of photon emission from an electron beam ion trap

D. W. Savin[1], M. F. Gu[1], and P. Beiersdorfer[2]

[1]Columbia Astrophysics Laboratory and Department of Physics, Columbia University, New York, NY 10027

[2] Department of Physics and Space Technology, Lawrence Livermore National Laboratory, Livermore, CA 94550

**Abstract**

**We present a theoretical formalism for calculating the anisotropy and polarization of photon emission due to a spiraling beam of electrons in an electron beam ion trap (EBIT). We present measurements of the polarization for the Fe XXIV $4p\ ^2P_{3/2} \rightarrow 2s\ ^2S_{1/2}$ X-ray transition due to electron impact excitation. We discuss these results, together with previously reported EBIT polarization measurements, in the light of electron spiraling. We find that spiraling effects cannot yet be discerned in these measurements. This is important for many EBIT measurements concerned with X-ray line intensity measurements. While the amount of spiraling is not accurately known, neglecting its effects introduces an error typically no larger than that given by counting statistics.**

## 1 Introduction

A unidirectional beam of electrons colliding with atomic or ionic targets may produce anisotropically emitted, partially polarized line radiation [1, 2, 3]. The emitted intensity from the target system depends upon the angle of observation relative to the axis defined by the beam. The measured intensity depends upon the angle of observation and whether or not the instrument used to analyze the emission is polarization sensitive. In this paper we discuss anisotropy and polarization issues relating to electron-ion collision studies which use an electron beam ion trap (EBIT) and detect the resulting photon emission. In particular we focus on the effect on the observed polarization of electron motion perpendicular to the electron beam direction.

EBITs use a magnetically confined, directed beam of unpolarized electrons to produce and trap an ensemble of unpolarized ions [4, 5, 6]. The theoretical formulae for calculating polarization of photon emission from an EBIT has been presented by Beiersdorfer *et al.* [7] for a unidirectional beam. The electrons in an

EBIT, however, are not truly unidirectional [7, 8, 9]. They possess a velocity component $\mathbf{v}_\perp$ which is perpendicular to the confining magnetic field $\mathbf{B}$. This produces spiraling along $\mathbf{B}$. The pitch angle $\theta$ is given by $\sin^2\theta = E_\perp/E$ where $E_\perp$ is the electron energy component due to $\mathbf{v}_\perp$ and $E$ is the total electron energy.

The average value of $E_\perp$ depends on the EBIT operating conditions, but we can estimate it for optimal operating conditions. The electron beam in an EBIT is formed in a region of low magnetic field strength. The $\mathbf{B}$ field in the trapping region is typically $\sim 3$ T. Using the principle of adiabatic invariants [10, 11] gives

$$E_\perp = E_{\perp c}\left(\frac{r_c}{r_b}\right)^2 = E_{\perp c}\left(\frac{B}{B_c}\right) \tag{1}$$

where $E_{\perp c}$ is the transverse energy of the electrons at the cathode, $r_c$ is the radius of the beam at the cathode, $r_b$ is the radius of the beam in the trapping region, and $B_c$ is the magnetic field strength at the cathode. $E_{\perp c}$ is roughly given by the cathode temperature $k_B T_c$ where $k_B$ is the Boltzmann constant and $T_c$ is the cathode temperature. For the Lawrence-Livermore EBIT, $r_c = 1.5$ mm, $r_b \sim 30$ $\mu$m and $k_B T_c \sim 0.1$ eV [4, 5, 7] which yields $E_\perp \sim 250$ eV. $E_\perp$ has also been estimated for the NIST EBIT [12] using two different techniques. The first technique used the electron cyclotron frequency as an upper limit on the rigid rotation of the beam, from which an estimate of $E_\perp \lesssim 700$ eV was derived [9]. The second technique involved a theoretical estimate of $B_c$. Takács *et al.* [9] derived a value of $B_c \sim 225$ $\mu$T. Their cathode temperature was $k_B T_c \sim 0.13$ eV and they find $E_\perp \sim 1700$ eV.

In this paper we investigate the effects of a non-vanishing value of $E_\perp$, *i.e.* of electron spiraling, on EBIT measurements. In Section 2 we use the theoretical formalism given by Stefan and Alder [13] to describe the photon emission from an EBIT taking spiraling into account. Section 3 discusses experiments to measure the polarization of the Fe XXIV $4p\ ^2P_{3/2} \rightarrow 2s\ ^2S_{1/2}$ transition produced by electron impact excitation (EIE). Section 4 discusses measurement uncertainties and presents our results. In Section 5 we discuss the results of our new polarization measurements as well as several previously reported EBIT polarization measurements [7, 8, 9] in the light of the effects of electron spiraling.

## 2 Theory

Here we develop theoretical expressions for the predicted angular distribution of photon emission from an EBIT. We are interested in collision processes which form an excited ion of initial total angular momentum $J_i$ which then radiatively decays to a final state of total angular momentum $J_f$. Our analysis follows the prescription of Steffen and Alder [13] and is valid for initial and final states of definite angular momentum.

We begin by defining three reference frames: the laboratory frame, the photon frame, and the electron frame. The relationship between the three is shown in Figures 1 and 2. In the laboratory frame $S$, $\mathbf{B}$ defines

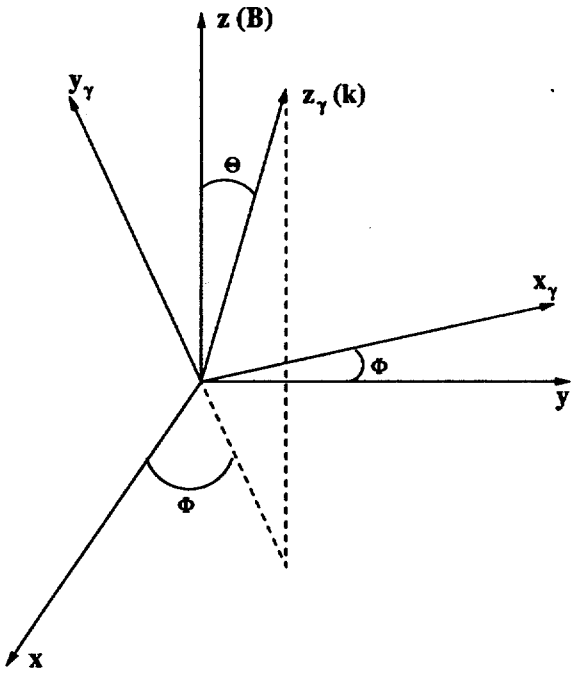


Figure 1: The relationship between the laboratory frame $S$ and the photon frame $S_\gamma$. The projection of the $z_\gamma$-axis onto the $xy$-plane is shown by the dashed lines. The $x_\gamma$-axis lies in the $xy$-plane.

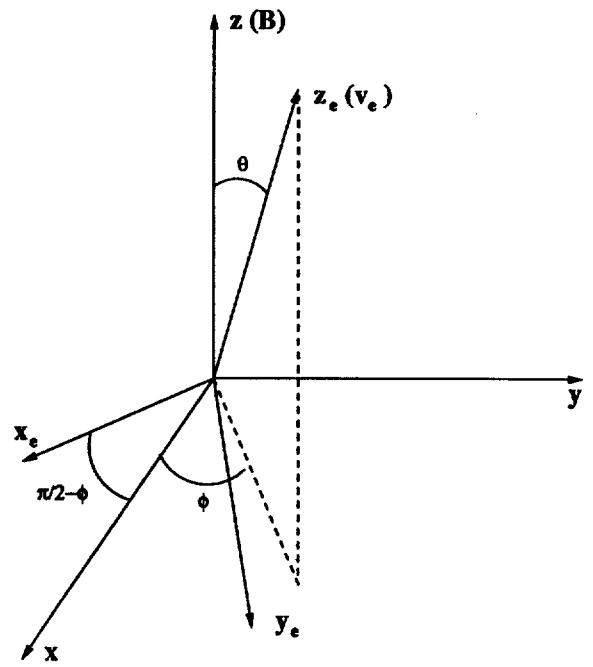


Figure 2: The relationship between the laboratory frame $S$ and the electron frame $S_e$. The projection of the $z_e$-axis onto the $xy$-plane is shown by the dashed lines. The $x_e$-axis lies in the $xy$-plane.

the $+z$-axis. In this frame, the directions of the electron velocity $\mathbf{v_e}$ and of the emitted photon $\mathbf{k}$ are given, respectively, by their polar angles $\theta$ and $\Theta$, and azimuthal angles $\phi$ and $\Phi$. The $+z$-axes of the photon frame $S_\gamma$ and the electron frame $S_e$ are determined by $\mathbf{k}$ and $\mathbf{v_e}$, respectively. The $+x$-axis of $S_\gamma$ is defined by $\mathbf{B} \times \mathbf{k}$. To bring $S$ to $S_\gamma$, a rotation $R(\Phi, \Theta, \pi/2)$ is performed, where $R(\alpha, \beta, \gamma)$ is the rotation operator expressed in Euler angles [14, 15]. We define the $+x$-axis of $S_e$ by $\mathbf{v_e} \times \mathbf{B}$. A rotation $R(-\pi/2, \theta, \pi - \phi)$ brings $S_e$ to $S$.

For radiative decays $i \to f$, the probability of detecting a photon emitted in the direction $\mathbf{k}$ using a detector with an efficiency matrix $\varepsilon$ is given by [13]

$$W(\mathbf{k}, \varepsilon) = \sum_{\tau,\tau'} < \tau|\rho_0^0(J_f)|\tau' >< \tau'|\varepsilon|\tau > (2J_f + 1)^{1/2} \tag{2}$$

where $< \tau|\rho_0^0(J_f)|\tau' >$ is the reduced matrix operator in the $S$ frame for a single photon process, $\rho_0^0(J_f)$ is a $2 \times 2$ matrix, and $\tau$ and $\tau'$ label photon helicity states. A label of $\tau$ or $\tau' = +1(-1)$ corresponds to left(right) circularly polarized light [14]. Re-expressing $< \tau|\rho_0^0(J_f)|\tau' >$ in terms of the statistical tensor before photon

emission, $\rho_q^\lambda(J_i)$, gives

$$
\begin{aligned}
< \tau|\rho_0^0(J_f)|\tau' > \;=\; & \frac{d\Omega}{8\pi} \sum_{LL'\lambda q} \frac{\begin{pmatrix} L & L' & \lambda \\ \tau & -\tau' & \mu \end{pmatrix}}{\begin{pmatrix} L & L' & \lambda \\ 1 & -1 & 0 \end{pmatrix}} \left(\frac{2J_i+1}{2J_f+1}\right)^{1/2} \rho_q^\lambda(J_i) \\
& \times[\gamma(EL)+\tau\gamma(ML)][\gamma^*(EL')+\tau'\gamma^*(ML')] \\
& \times F_\lambda(LL'J_fJ_i) D_{q\mu}^{(\lambda)*}(S\to S_\gamma) \Big/ \sum_{L\pi} |\gamma(\pi L)|^2. \qquad (3)
\end{aligned}
$$

Here $L$ is the order of what Steffen and Alder call a pure $2^L$ multipole decay; the quantities in the large parenthesis denote Wigner 3-$j$ symbols; and $\gamma(\pi L)$ is the multipole transition amplitude with $\pi = E(M)$ for electric(magnetic) transitions. $F_\lambda(LL'J_fJ_i)$ is given by

$$
F_\lambda(LL'J_fJ_i) = (-1)^{J_f+J_i-1}[(2\lambda+1)(2L+1)(2L'+1)(2J_i+1)]^{1/2} \begin{pmatrix} L & L' & \lambda \\ 1 & -1 & 0 \end{pmatrix} \begin{Bmatrix} L & L' & \lambda \\ J_i & J_i & J_f \end{Bmatrix} \qquad (4)
$$

where the quantity in the large braces denotes a Wigner 6-$j$ symbol. The properties and values of the 3-$j$ and 6-$j$ symbols are given by Cowan [16]. $D_{q\mu}^{(\lambda)*}(S\to S_\gamma) = D_{q\mu}^{(\lambda)*}(\Phi,\Theta,\pi/2)$ is the rotation matrix from $S$ to $S_\gamma$. The rotation matrices are described in detail in Refs. [14] and [15].

EBIT measurements commonly use detectors which are sensitive to linearly polarized radiation. For these detectors, the efficiency matrix in the representation of helicity states is given by [13]

$$
\varepsilon = \frac{\mathcal{E}}{2} \begin{pmatrix} 1 & -Qe^{-i2\alpha} \\ -Qe^{i2\alpha} & 1 \end{pmatrix} \qquad (5)
$$

where $\mathcal{E}$ is the total efficiency of the detector; $\alpha$ is the angle between the polarization axis of the detector and the $x_\gamma$-axis; and $Q$ is the linear polarization efficiency. We define the efficiency for radiation polarized along the polarization axis of the detector as $\mathcal{E}_p = \frac{\mathcal{E}}{2}(1+Q)$ and perpendicular to the polarization axis as $\mathcal{E}_s = \frac{\mathcal{E}}{2}(1-Q)$. The efficiency matrix may now be written as

$$
\varepsilon = \frac{1}{2} \begin{pmatrix} \mathcal{E}_s+\mathcal{E}_p & (\mathcal{E}_s-\mathcal{E}_p)e^{-i2\alpha} \\ (\mathcal{E}_s-\mathcal{E}_p)e^{i2\alpha} & \mathcal{E}_s+\mathcal{E}_p \end{pmatrix}. \qquad (6)
$$

A straightforward manipulation of Equation 3 gives

$$
< \tau|\rho_0^0(J_f)|\tau > \;=\; \frac{d\Omega}{8\pi} \left(\frac{2J_i+1}{2J_f+1}\right)^{1/2} \sum_{\lambda q} \tau^\lambda \rho_q^\lambda(J_i) A_\lambda^\pm D_{q0}^{(\lambda)*}(S\to S_\gamma) \qquad (7)
$$

$$
< \tau|\rho_0^0(J_f)|-\tau > \;=\; \frac{d\Omega}{8\pi} \left(\frac{2J_i+1}{2J_f+1}\right)^{1/2} \sum_{\lambda q} \tau^\lambda \rho_q^\lambda(J_i) A_{\lambda,2}^\pm D_{q\mp 2}^{(\lambda)*}(S\to S_\gamma). \qquad (8)
$$

$A_\lambda^+$, $A_{\lambda,2}^+$, and $D_{q-2}^{(\lambda)*}$ ($A_\lambda^-$, $A_{\lambda,2}^-$, and $D_{q2}^{(\lambda)*}$) correspond to $\tau = +1(-1)$ and

$$
A_\lambda^+ \;=\; \sum_{L\pi L'\pi'} F_\lambda(LL'J_fJ_i)\gamma(\pi L)\gamma^*(\pi' L') \Big/ \sum_{L\pi} |\gamma(\pi L)|^2 \qquad (9)
$$

$$A_\lambda^- = \sum_{L\pi L'\pi'} (-1)^{L+L'+\Lambda(\pi)+\Lambda(\pi')} F_\lambda(LL'J_fJ_i)\gamma(\pi L)\gamma^*(\pi' L') \Big/ \sum_{L\pi} |\gamma(\pi L)|^2 \tag{10}$$

$$A_{\lambda,2}^+ = \sum_{L\pi L'\pi'} (-1)^{\Lambda(\pi')} \frac{\begin{pmatrix} L & L' & \lambda \\ 1 & 1 & -2 \end{pmatrix}}{\begin{pmatrix} L & L' & \lambda \\ 1 & -1 & 0 \end{pmatrix}} F_\lambda(LL'J_fJ_i)\gamma(\pi L)\gamma^*(\pi' L') \Big/ \sum_{L\pi} |\gamma(\pi L)|^2 \tag{11}$$

$$A_{\lambda,2}^- = \sum_{L\pi L'\pi'} (-1)^{L+L'+\Lambda(\pi)} \frac{\begin{pmatrix} L & L' & \lambda \\ 1 & 1 & -2 \end{pmatrix}}{\begin{pmatrix} L & L' & \lambda \\ 1 & -1 & 0 \end{pmatrix}} F_\lambda(LL'J_fJ_i)\gamma(\pi L)\gamma^*(\pi' L') \Big/ \sum_{L\pi} |\gamma(\pi L)|^2 \tag{12}$$

where $\Lambda(E) = 0$ and $\Lambda(M) = 1$. It can be shown that $A_\lambda^{\pm *} = A_\lambda^\pm$ and $A_{\lambda,2}^{\pm *} = (-1)^\lambda A_{\lambda,2}^\mp$, which ensures that $\rho_0^0(J_f)$ is hermitian. Symetry under time reversal implies the transition amplitudes $\gamma(\pi L)$ are all real or all pure imaginary [14]. So $A_{\lambda,2}^\pm$ is real and $A_{\lambda,2}^\pm = (-1)^\lambda A_{\lambda,2}^\mp$. The angular distribution factor can now be written

$$\begin{aligned} W(\Phi,\Theta,\alpha,\mathcal{E}_p,\mathcal{E}_s) &= \frac{d\Omega}{16\pi} \sum_{\lambda q} (2J_i+1)^{1/2} \rho_q^\lambda(J_i) \\ &\times \Bigg\{ (\mathcal{E}_p+\mathcal{E}_s)(A_\lambda^+ + (-1)^\lambda A_\lambda^-) \left(\frac{4\pi}{2\lambda+1}\right)^{1/2} Y_{\lambda q}^*(\Theta,\Phi) \\ &-(\mathcal{E}_p-\mathcal{E}_s)\Big[A_{\lambda,2}^+ D_{q-2}^{(\lambda)*}(\Phi,\Theta,\pi/2+\alpha) \\ &+(-1)^\lambda A_{\lambda,2}^- D_{q2}^{(\lambda)*}(\Phi,\Theta,\pi/2+\alpha)\Big]\Bigg\}. \end{aligned} \tag{13}$$

Here we have used [15]

$$D_{q0}^{(\lambda)*}(\Phi,\Theta,\pi/2) = \left(\frac{4\pi}{2\lambda+1}\right)^{1/2} Y_{\lambda q}^*(\Theta,\Phi) \tag{14}$$

where $Y_{\lambda q}$ is the spherical harmonic and

$$D_{q\pm 2}^{(\lambda)*}(\Phi,\Theta,\pi/2+\alpha) = D_{q\pm 2}^{(\lambda)*}(\Phi,\Theta,\pi/2)e^{\pm i2\alpha}. \tag{15}$$

The radiating system is formed by an electron colliding with a quasistationary ion. In this, the $S_e$ frame, the system is axisymmetric along $\mathbf{v_e}$ and the initial statistical tensor $\rho_q'^\lambda$ is nonzero only for $q = 0$. The statistical tensors in $S$ and $S_e$ are related by the rotation

$$\begin{aligned} \rho_q^\lambda(J_i,\theta,\phi) &= \sum_{q'} \rho_{q'}'^\lambda(J_i) D_{q'q}^{(\lambda)*}(-\pi/2,\theta,\pi-\phi) \\ &= \rho_0'^\lambda(J_i) D_{0q}^{(\lambda)*}(-\pi/2,\theta,\pi-\phi) \end{aligned} \tag{16}$$

where

$$\rho_0'^\lambda(J_i) = \sum_m (-1)^{J_i+m}(2\lambda+1)^{1/2} \begin{pmatrix} J_i & J_i & \lambda \\ -m & m & 0 \end{pmatrix} g_m. \tag{17}$$

The factor $g_m$ represents the population density of the magnetic sublevel $m$. The $m$ values are quantized along $\mathbf{v}_e$. The density matrix $\rho'$ is normalized so that $\mathrm{Tr}\rho' = \sum_m g_m = 1$. It is convenient to introduce the orientation parameters which are defined as

$$B_\lambda(J_i) = (2J_i + 1)^{1/2} \rho_0'^\lambda(J_i). \tag{18}$$

The density matrix is normalized so that $B_0$=1.

The electrons in an EBIT can be described by a pitch angle distribution $f(\cos\theta)$, which we normalize so that $\int_{-1}^{1} d(\cos\theta) f(\cos\theta) = 1$. The electrons travel along the $\sim$ 3 T magnetic field lines in the trapping volume, spiraling incoherently with a cyclotron frequency of $\sim 5.3 \times 10^{11}$ revolutions $\mathrm{s}^{-1}$. For kinetic energies $\lesssim$ 100 keV, the electrons undergo $\gtrsim$25 revolutions as they traverse the observed central 1 cm length of the trap. This large number of revolutions allows us to calculate the initial statistical tensor of the radiating system by averaging Equation 16 over $\theta$ and $\phi$. This gives

$$\begin{aligned} \rho_q^\lambda(J_i) &= \int_{-1}^{1} d(\cos\theta) f(\cos\theta) \int_0^{2\pi} \frac{d\phi}{2\pi} \rho_q^\lambda(J_i, \theta, \phi) \\ &= \rho_0'^\lambda(J_i) \int_{-1}^{1} d(\cos\theta) f(\cos\theta) \int_0^{2\pi} \frac{d\phi}{2\pi} D_{0q}^{(\lambda)*}(-\pi/2, \theta, \pi - \phi) \\ &= \delta_{q0} g_\lambda \rho_q'^\lambda(J_i) \end{aligned} \tag{19}$$

where

$$g_\lambda = \int_{-1}^{1} d(\cos\theta) f(\cos\theta) P_\lambda(\cos\theta) \tag{20}$$

and $P_\lambda(\cos\theta)$ is the Legendre polynomial. Using Equations 13, 18, and 19 yields the angular distribution factor for radiation produced by a spiraling beam of electrons,

$$\begin{aligned} W(\Phi, \Theta, \alpha, \mathcal{E}_p, \mathcal{E}_s) &= \frac{d\Omega}{16\pi} \sum_\lambda g_\lambda B_\lambda \Big\{ (\mathcal{E}_p + \mathcal{E}_s)(A_\lambda^+ + (-1)^\lambda A_\lambda^-) P_\lambda(\cos\Theta) - (\mathcal{E}_p - \mathcal{E}_s) \\ &\quad \times \Big[ A_{\lambda,2}^+ D_{0-2}^{(\lambda)*}(\Phi, \Theta, \pi/2 + \alpha) + (-1)^\lambda A_{\lambda,2}^- D_{02}^{(\lambda)*}(\Phi, \Theta, \pi/2 + \alpha) \Big] \Big\}. \end{aligned} \tag{21}$$

Here we have used

$$\left( \frac{4\pi}{2\lambda + 1} \right)^{1/2} Y_{\lambda 0}^*(\Theta, \Phi) = P_\lambda(\cos\Theta). \tag{22}$$

Parity is typically a good quantum number for atomic states. When this is true, the multipole transition amplitudes $\gamma(\pi L)$ and $\gamma(\pi' L')$, which link the same initial and final states, vanish unless

$$\pi_i \pi_f = (-1)^{L + \Lambda(\pi)} = (-1)^{L' + \Lambda(\pi')} \tag{23}$$

where $\pi_i$ and $\pi_f$ are the parities of the initial and final states [14]. This ensures that $(-1)^{L + L' + \Lambda(\pi) + \Lambda(\pi')} = 1$. We can now define the angular distribution coefficients $A_\lambda$ and $A_{\lambda,2}$ as

$$A_\lambda \equiv A_\lambda^+ = A_\lambda^- \tag{24}$$

$$A_{\lambda,2} \equiv A^{+}_{\lambda,2} = A^{-}_{\lambda,2}. \tag{25}$$

Since $A_{\lambda,2} = (-1)^{\lambda} A_{\lambda,2}$, it vanishes for $\lambda = odd$. $A_\lambda$ is normalized so that $A_0 = 1$. The rotation matrix elements $D^{(\lambda)*}_{0\pm 2}$ can be expressed [15, 17]

$$D^{(\lambda)*}_{0\pm 2}(\Phi, \Theta, \pi/2 + \alpha) = -\left(\frac{(\lambda-2)!}{(\lambda+2)!}\right)^{1/2} P^{(2)}_{\lambda}(\cos\Theta) e^{\mp i 2\alpha} \tag{26}$$

where $P^{(2)}_{\lambda}(\cos\Theta)$ is the associated Legendre polynomial. Using Equations 21, 24, 25, and 26 gives

$$\begin{aligned} W(\Phi, \Theta, \alpha, \mathcal{E}_p, \mathcal{E}_s) &= \frac{d\Omega}{8\pi} \sum_{\lambda=even} g_\lambda B_\lambda \Big[ (\mathcal{E}_p + \mathcal{E}_s) A_\lambda P_\lambda(\cos\Theta) \\ &\quad + (\mathcal{E}_p - \mathcal{E}_s) A_{\lambda,2} \left(\frac{(\lambda-2)!}{(\lambda+2)!}\right)^{1/2} P^{(2)}_{\lambda}(\cos\Theta)\cos 2\alpha \Big]. \end{aligned} \tag{27}$$

The above derivation is valid for an admixture of multipole transitions. For atomic systems, the approximation of transitions as single multipole operators is accurate so long as $(\alpha Z_{eff})^2 \ll 1$, where $\alpha$ is the fine structure constant and $Z_{eff}$ is the effective nuclear charge of the ion [18]. In this approximation, $L = L'$ and the angular distribution coefficients become

$$A_\lambda = F_\lambda(LLJ_fJ_i) \tag{28}$$

$$A_{\lambda,2} = (-1)^{\Lambda(\pi)} \frac{\begin{pmatrix} L & L & \lambda \\ 1 & 1 & -2 \end{pmatrix}}{\begin{pmatrix} L & L & \lambda \\ 1 & -1 & 0 \end{pmatrix}} A_\lambda. \tag{29}$$

The angular distribution factor can now be written

$$\begin{aligned} W(\Theta, \alpha, \mathcal{E}_p, \mathcal{E}_s) &= \frac{d\Omega}{8\pi} \sum_{\lambda=even} g_\lambda A_\lambda B_\lambda \Big[ (\mathcal{E}_p + \mathcal{E}_s) P_\lambda(\cos\Theta) \\ &\quad - (\mathcal{E}_p - \mathcal{E}_s) f_\lambda(L) P^{(2)}_{\lambda}(\cos\Theta)\cos 2\alpha \Big] \end{aligned} \tag{30}$$

where

$$f_\lambda(L) = -(-1)^{\Lambda(\pi)} \left(\frac{(\lambda-2)!}{(\lambda+2)!}\right)^{1/2} \frac{\begin{pmatrix} L & L & \lambda \\ 1 & 1 & -2 \end{pmatrix}}{\begin{pmatrix} L & L & \lambda \\ 1 & -1 & 0 \end{pmatrix}}. \tag{31}$$

Taking $\mathcal{E}_p(\mathcal{E}_s) = 1(0)$ and $\mathcal{E}_p(\mathcal{E}_s) = 0(1)$, the emitted angular distribution along the $p$ and $s$ axes of the detector, is given, respectively, by

$$W_{p(s)}(\Theta, \alpha) = \frac{d\Omega}{8\pi} \sum_{\lambda=even} g_\lambda A_\lambda B_\lambda \left[ P_\lambda(\cos\Theta) \mp f_\lambda(L) P^{(2)}_{\lambda}(\cos\Theta)\cos 2\alpha \right] \tag{32}$$

where the $-(+)$ corresponds to the $p(s)$ polarization component of the radiation. The polarization factor $P(\Theta, \alpha)$ can be defined

$$P(\Theta, \alpha) = \frac{W_s(\Theta, \alpha) - W_p(\Theta, \alpha)}{W_s(\Theta, \alpha) + W_p(\Theta, \alpha)}$$

$$= \cos 2\alpha \frac{\sum_{\lambda=even} f_\lambda(L) P_\lambda^{(2)}(\cos\Theta) g_\lambda B_\lambda A_\lambda}{\sum_{\lambda=even} P_\lambda(\cos\Theta) g_\lambda B_\lambda A_\lambda}. \tag{33}$$

For a non-spiraling beam, $\Theta = \pi/2$, and $\alpha = 0$, this matches with the standard definition of the polarization factor [1, 2, 3]. Equation 30 can now be expressed in terms of $P(\Theta, \alpha)$ as

$$W(\Theta, \alpha, \mathcal{E}_p, \mathcal{E}_s) = \frac{d\Omega}{8\pi}\Big[(\mathcal{E}_s + \mathcal{E}_p) + (\mathcal{E}_s - \mathcal{E}_p)P(\Theta, \alpha)\Big] \sum_{\lambda=even} P_\lambda(\cos\Theta) g_\lambda A_\lambda B_\lambda \tag{34}$$

For a polarization insensitive detector, $\mathcal{E}_p = \mathcal{E}_s = \mathcal{E}/2$, and

$$W(\Theta) = \frac{\mathcal{E} d\Omega}{4\pi} \sum_{\lambda=even} g_\lambda A_\lambda B_\lambda P_\lambda(\cos\Theta). \tag{35}$$

The vast majority of EBIT measurements involve the detection of dipole radiation ($L = 1$) using photon detectors placed so that $\Theta = \pi/2$ and $\alpha = 0$. For this situation

$$P = \frac{\mp 3 g_2 A_2 B_2}{2 - g_2 A_2 B_2}. \tag{36}$$

Here we have used

$$\begin{aligned} P_0(0) &= +1 \\ P_2(0) &= -\frac{1}{2} \\ P_2^{(2)}(0) &= +3 \\ f_2(1) &= \mp\frac{1}{2} \\ g_0 = A_0 = B_0 &= +1 \end{aligned}$$

where $-(+)$ corresponds to electric(magnetic) dipole radiation. We define $P = \mathcal{P}$ for situations where the pitch angle of the electrons $\theta = 0$, in which case $g_\lambda = 1$ and

$$\mathcal{P} = \frac{\mp 3 A_2 B_2}{2 - A_2 B_2}. \tag{37}$$

Re-writing equation 37 in terms of $A_2 B_2$ gives

$$A_2 B_2 = \frac{2\mathcal{P}}{\mathcal{P} \mp 3}. \tag{38}$$

$P$ can now expressed in terms of $\mathcal{P}$ as

$$P = \mathcal{P} \frac{3 g_2}{3 \mp (1 - g_2)\mathcal{P}}. \tag{39}$$

If the electrons have an arbitrary fixed pitch angle $\theta_0$, *i.e.* $f(\cos\theta) = \delta(\cos\theta - \cos\theta_0)$, then

$$\begin{aligned} g_2 &= -\frac{1}{2} + \frac{3}{2}\cos^2\theta_0 \\ &= 1 - \frac{3}{2}\epsilon \end{aligned} \tag{40}$$

where $\epsilon = \sin^2\theta_0 = E_\perp/E$. The polarization of photon emission from an EBIT is then given by

$$P = \mathcal{P}\frac{2-3\epsilon}{2 \mp \epsilon\mathcal{P}} \tag{41}$$

and the angular distribution factor by

$$W(\mathcal{E}_p, \mathcal{E}_s) = \frac{d\Omega}{8\pi}\left[(\mathcal{E}_s + \mathcal{E}_p) + (\mathcal{E}_s - \mathcal{E}_p)P\right]\frac{3}{3 \mp P}. \tag{42}$$

Thus we find for dipole radiation that if $f(\cos\theta) = \delta(\cos\theta - \cos\theta_0)$ accurately describes the electron pitch angle distribution, then the effect of electron spiraling on the anisotropy and polarization of the emitted radiation can be fully and easily accounted for using only the pitch angle $\theta_0$ and the polarization $\mathcal{P}$ for a non-spiraling electron beam.

The upper level in the $i \to f$ decay may sometimes be populated by cascades from a higher-lying excited level. The effect of cascades on the predicted emission is calculated through the use of the de-orientation factor as described by Stefan and Alder [13] and applied to atomic transitions by Beiersdorfer *et al.* [7]. This factor is unaffected by electron spiraling.

# 3 Experimental Technique

The electron density in the Lawrence-Livermore EBITs [4, 5, 19] can be varied between $\sim 10^{11} - 10^{13}$ cm$^{-3}$. The energy spread of the electron beam for typical operating parameters is $\Delta E \sim 50$ eV [5, 20]. For typical measurement energies $\Delta E/E << 1$ and the beam energy can be approximated as monoenergetic. In this approximation, the total line formation rate can be written

$$I = \sigma(E)v_e(E)\int n_e(\mathbf{r})n_q(\mathbf{r})d^3\mathbf{r} \tag{43}$$

where $\sigma$ is the total cross section for collisionally producing the line of interest and includes cascade contributions; $n_e(\mathbf{r})$ is the electron density at $\mathbf{r}$; $n_q(\mathbf{r})$ is the density at $\mathbf{r}$ of ions in charge state $q$ of the element of interest; and $\int d^3\mathbf{r}$ is over the volume of the trap. Excited ions are assumed to radiatively decay on a time scale significantly shorter than either the trapping time of the ions or the timescale over which the charge balance in the trap may change.

The diameter of the electron beam in EBIT is $\sim 60$ $\mu$m [5]. The attractive potential of the electron beam and the applied magnetic field confine the ions in the radial direction. The temperature of the ions is $\sim 600$ eV for operating parameters typically used for EBIT spectroscopy measurements [21, 22]. If the radiative lifetime of the excited ions is $\lesssim 10^{-9}$ s, then the excited ions will radiatively decay primarily within

the confines of the electron beam. Photon emission from EBIT is thus similar to that from an entrance slit for a spectrometer.

We have used a flat crystal spectrometer (FCS) [23, 24], for the present measurements. Crystal spectrometers are polarization sensitive instruments. The reflectivity of a crystal is different for photons polarized perpendicular to the dispersion plane ($s$-polarized) and for photons polarized in the dispersion plane ($p$-polarized) [25, 26]. The dispersion plane of the FCS on EBIT is perpendicular to the magnetic field that confines the electrons (*i.e.*, $\Theta = \pi/2$ and $\alpha = 0$). The FCS views the central $\sim$ 1 cm length of the trap. Between EBIT and the FCS is a 4$\mu$m thick polypropelene window. X-rays are detected using a flowing gas proportional counter [27] with a 4$\mu$m thick polypropelene window. There is a continuous flow of 90% Ar and 10% $CH_4$ at a constant pressure of $\sim$ 1 atmosphere. A series of vertical apertures collimate the observed emission for a maximum divergence of $\lesssim$ 18 milliradians in the vertical dimension. In the horizontal dimension the angular width of the collected radiation overfills the angular acceptance angle of the crystals used.

The intensity of a dipole transition as measured using a crystal spectrometer can be calculated by multiplying Equations 42 and 43. $W$ is essentially constant over the solid angle collected by the crystal spectrometer (CS). So, setting $\mathcal{E}_p = TD\psi R_p$ and $\mathcal{E}_s = TD\psi R_s$, we have

$$I^{CS} = \frac{3TD\psi[(R_s + R_p) + (R_s - R_p)P]}{2(3 \mp P)} \left(\frac{I}{4\pi}\right) \tag{44}$$

where $T$ accounts for all window transmittances, $D$ is the detection efficiency of the proportional counter, $\psi$ is the effective vertical angle collected by the spectrometer, and $R_s$ and $R_p$ are the integrated reflectivities of the crystal for radiation polarized, respectively, perpendicular to and parallel to the dispersion plane. The solid angle $d\Omega$ is implicitly accounted for in the terms $\psi R_s$ and $\psi R_p$.

Polarization measurements of dipole transitions are carried out using a crystal spectrometer and simultaneously observing two lines, $a$ and $b$, with nearly identical Bragg angles. If the two line are emitted by the same charge state, then the measured line ratio will be independent of $\int n_e n_q d^3\mathbf{r}$. Assuming that $T$, $A$, $R_s$, and $R_p$ are essentially constant over the range of Bragg angles spanned by the two lines, then we may use Equations 43 and 44 to write

$$\frac{I_a^{CS}}{I_b^{CS}} = \frac{[1 + f + (1 - f)P_a]\sigma_a}{[1 + f + (1 - f)P_b]\sigma_b} \tag{45}$$

where $f = R_p/R_s$. Polarization factors are determined by observing the same pair of lines with two different

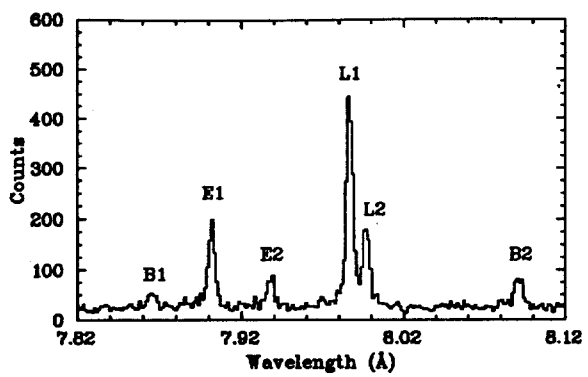


Figure 3: Iron spectrum recorded at an electron beam energy of 4.6 keV. The spectrum was collected over $\sim$ 26 hours using an ammonium dihydrogen phosphate (101) crystal in first order. Lines are labeled using the notation of Table 1.

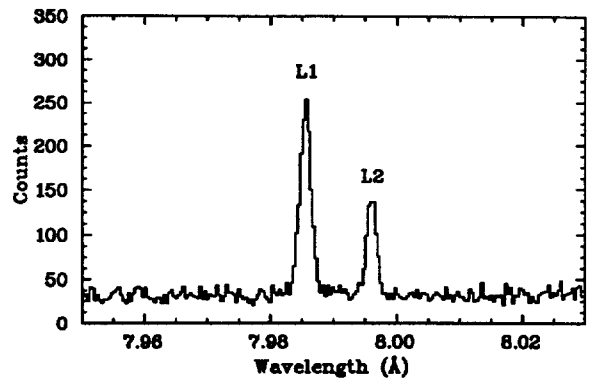


Figure 4: Iron spectrum recorded at an electron beam energy of 4.6 keV. The spectrum was collected over $\sim$ 27 hours using an $\alpha$-quartz $(10\bar{1}0)$ crystal in first order. Lines are labeled using the notation of Table 1.

| Label | Fe Ion | Transition | $\lambda$ (Å) |
|---|---|---|---|
| B1 | XXII | $2s^2 2p\ ^2P_{1/2} - 2s2p_{1/2}5p_{1/2,3/2}$ | 7.865 |
| E1 | XXIII | $2s2p\ ^1P_1 - 2s5d\ ^1D_2$ | 7.901 |
| E2 | XXIII | $2s2p\ ^1P_1 - 2s5s\ ^1S_0$ | 7.936 |
| L1 | XXIV | $2s\ ^2S_{1/2} - 4p\ ^2P_{3/2}$ | 7.986 |
| L2 | XXIV | $2s\ ^2S_{1/2} - 4p\ ^2P_{1/2}$ | 7.996 |
| B2 | XXII | $2s^2 2p\ ^2P_{1/2} - 2s^2 5d\ ^2D_{3/2}$ | 8.091 |

Table 1: Observed iron spectral lines. Line identifications and wavelengths come from Wargelin *et al.* [28]. The labeling convention is L for Li-like Fe XXIV, E for Be-like Fe XXIII, and B for B-like Fe XXII

crystals. Using Equation 45 for the two different crystals, 1 and 2, $P_a$ can be expressed in terms $P_b$ as

$$P_a = \frac{\left(\frac{I_a}{I_b}\right)_2 \left(f_1+1\right)\left(\frac{1-P_b}{1+P_b} f_2 + 1\right) - \left(\frac{I_a}{I_b}\right)_1 \left(f_2+1\right)\left(\frac{1-P_b}{1+P_b} f_1 + 1\right)}{\left(\frac{I_a}{I_b}\right)_2 \left(f_1-1\right)\left(\frac{1-P_b}{1+P_b} f_2 + 1\right) - \left(\frac{I_a}{I_b}\right)_1 \left(f_2-1\right)\left(\frac{1-P_b}{1+P_b} f_1 + 1\right)}. \tag{46}$$

where we have dropped the $CS$ superscript for convenience. Equation 46 simplifies somewhat if the $J_i = 1/2$ for line $b$. For this situation, $B_\lambda(1/2)$ is nonzero only for $\lambda \leq 1$ so that $P_b = 0$.

# 4 Measurement

Measurement of the Fe XXIV $4p\ ^2P_{3/2} - 2s\ ^2S_{1/2}$ polarization produced by EIE were carried out by measuring its intensity relative to that of the $4p\ ^2P_{1/2} - 2s\ ^2S_{1/2}$ transition using two different crystals. Since $J_i = 1/2$ for the $4p\ ^2P_{1/2} - 2s\ ^2S_{1/2}$ transition, the line is unpolarized and thus provides an ideal polarization reference.

Representative iron spectra collected for the present results are shown in Figures 3 and 4. Figure 3 was obtained using an ammonium dihydrogen phosphate [ADP (101)] crystal and Figure 4 using an $\alpha$-

quartz $(10\bar{1}0)$ crytsal. All spectra were collected in first order. Line ratios were determined using the fitted integrated line intensities. Observed lines are listed in Table 1. Line identifications and wavelengths are from Wargelin *et al.* [28]. The spectra consist entirely of lines due to Fe XXII, XXIII, and XXIV. Spectra collected when no iron ions were in the trap were devoid of any discernable spectral lines. Contamination of the observed spectra from elements other than iron is thus believed to be insignificant.

Observed line intensities may be affected by recombination-cascade processes such as charge transfer (CT) with background gas molecules or radiative recombination (RR) with either beam electrons or low energy background electrons. The effects of CT and RR on Fe XXIV EIE produced $(3p\,^2P_{3/2} - 2s\,^2S_{1/2})/(3p\,^2P_{1/2} - 2s\,^2S_{1/2})$ and $(4p\,^2P_{3/2,1/2} - 2s\,^2S_{1/2})/(3p\,^2P_{1/2} - 2s\,^2S_{1/2})$ line ratio measurements was investigated by Savin *et al.* [29] and found to be insignificant. By inference, we assume that both CT and RR have an insignificant effect on the measured $(4p\,^2P_{3/2} - 2s\,^2S_{1/2})/(4p\,^2P_{1/2} - 2s\,^2S_{1/2})$ line ratios.

Measured line ratios were reproducible to within 5 to 7 percent. This is slightly greater than predicted by $1\sigma$ counting statistics and is attributed as to variations introduced when determining the background levels of the collected spectra. The resulting uncertainties in the measured polarization factors were determined by calculating the variance of Equation 46 [30].

The value used in Equation 46 for $f$ depends on the Bragg angle, $\theta_B$, of the observed line. The Bragg angle was calculated using the measured wavelengths of the Fe XXIV lines [28] and the measured $2d_\infty$ spacing for $\alpha$-quartz $(10\bar{1}0)$ [31, 32] and ADP (101) crystals [33, 34]. Uncertainties in the measured wavelengths and $2d_\infty$ spacings have an insignificant effect on the present results.

The values of $f$ used were determined from theoretical considerations and the reported measured properties of $\alpha$-quartz and ADP. For a perfect crystal with negligible absorption, $f = |\cos(2\theta_B)|$; but for a perfect crystal with with non-negligible absorption, $f$ may be significantly less. For a mosaic crystal $f = \cos^2(2\theta_B)$ [25, 26]. The properties of $\alpha$-quartz $(10\bar{1}0)$ deviates from those of a perfect crystal at $\sim 8$ Å (roughly the wavelength of the Fe XXIV $4p - 2s$ lines) [35]. The value of $f_{quartz}$ at $\sim 8$ Å is bounded by the theoretical values of 0.764 for a perfect crystal and 0.584 for a mosaic crystal. ADP is a crystal with a significant amount of absorption [26]. The value of $f_{ADP}$ at $\sim 8$ Å is bounded by the theoretical values of 0.046 for a perfect crystal with absorption [26] and 0.016 for a mosaic crystal. We used the limits on the theoretical values of $f_{quartz}$ and $f_{ADP}$ to calculate average values which we then used in the Equation 46. Using the uncertainties in $f$ for the different crystals, we determined the resulting uncertainties in the measured polarization factors by calculating the variance of Equation 46.

Table 2 lists the uncertainties associated with the $4p\,^2P_{3/2} - 2s\,^2S_{1/2}$ polarization measurement. Uncer-

| Source | 2.5 keV | 4.6 keV |
|---|---|---|
| Line intensity measurements using: | | |
| $\alpha$-quartz($10\bar{1}0$) | 0.089 | 0.147 |
| ADP(101) | 0.094 | 0.101 |
| Theoretical $f$ values: | | |
| $\alpha$-quartz($10\bar{1}0$) | 0.008 | 0.050 |
| ADP(101) | 0.003 | 0.012 |
| Quadrature Sum | 0.130 | 0.186 |

Table 2: Summary of uncertainties for Fe XXIV $4p\ ^2P_{3/2} \rightarrow 2s\ ^2S_{1/2}$ polarization measurements. All uncertainties are quoted at a confidence level believed to be equivalent to a $1\sigma$ confidence level.

tainties are quoted at a confidence level believed to be equivalent to a $1\sigma$ statistical confidence level. The uncertainties are treated as random sign errors and added in quadrature.

The measured polarization factors of Fe XXIV $4p\ ^2P_{3/2} \rightarrow 2s\ ^2S_{1/2}$ line emission produced by EIE at collision energies of 2.5 and 4.6 keV are shown in Figure 5. The error bars represent the estimated $1\sigma$ uncertainties.

# 5 Discussion

In order to estimate the effect of electron spiraling on the measured polarization of the Fe XXIV $4p\ ^2P_{3/2} \rightarrow 2s\ ^2S_{1/2}$ transition, we plot in Figure 5 the theoretical polarization factors as a function of collision energy for $E_\perp = 0$, 250, and 700 eV. We have assumed that $f(\cos\theta) = \delta(\cos\theta - \cos\theta_0)$. The collision energy was above the ionization potential for Fe XXIV [36] and cascades contributed to the observed $4p - 2s$ lines intensities. A relativistic distorted wave code was used to calculate the population of the magnetic sublevels $m$ due to electron impact excitation [37]. Radiative rates and cascades branching ratios were calculated using a multiconfiguration, relativisitic, parametric potential method in intermediate coupling [38]. Using these theoretical atomic data, a collisional-radiative model was constructed to determine the $g_m$ values for the initial statistical tensor $\rho_0^\lambda$ (*cf.* Equation 17). Cascade contributions to the theoretical polarization were account for as described in Beiersdorfer *et al.* [7].

As can be seen in Figure 5, the present results are in reasonable agreement with theory. The agreement does not depend on whether or not spiraling has been taken into account. This is a result of three factors: the relatively small value of $E_\perp/E$ for the energies at which the measurement were carried out, the moderate polarization of the lines, and the large error bars.

Polarization measurements using the present technique involve subtraction (*cf.* Equation 46). To produce polarization measurements with small relative uncertainties requires that the uncertainties in the values being

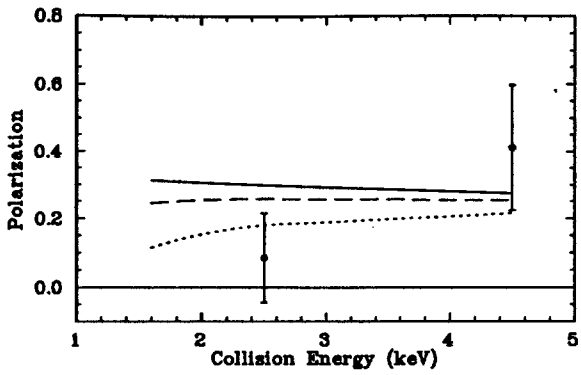


Figure 5: Measured and theoretical Fe XXIV $4p\ ^2P_{3/2} \rightarrow 2s\ ^2S_{1/2}$ polarization factor. The measured values are shown with their estimated $1\sigma$ uncertainties. The theoretical values are shown for $E_\perp = 0$ eV (solid line), 250 eV (dashed line), and 700 eV (dotted line).

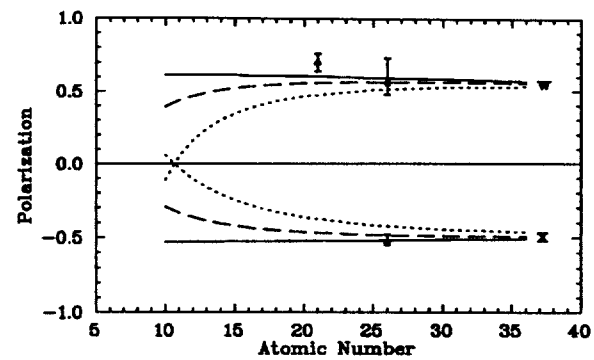


Figure 6: Measured and theoretical polarization factors for $1s2p\ ^1P_1 \rightarrow 1s^2\ ^1S_1$ ($w$) and $1s2p\ ^3P_2 \rightarrow 1s^2\ ^1S_1$ ($x$) line emission in heliumlike ions produced by electron impact excitation at threshold. The measured value for Sc XX (triangle) is from Henderson *et al.* [8] and for Fe XXV (circles) from Beiersdorfer *et al.* [7]. The $E_\perp = 0$ eV theoretical values are from Beiersdorfer *et al.* Also shown are the theoretical polarization factors for $E_\perp = 250$ eV (dashed line) and 700 eV (dotted line).

subtracted be extremely small. Meeting this requirement is often limited by counting statistics which only improve as the square root of the data acquisition time. One quickly runs into the limits of diminishing returns. This means that the effect of electron spiraling in many cases will not be significant. Uncertainties determined by statistics will typically be larger than the effect of spiraling. This was also noted in Refs. [7], [8] and [9] and now is confirmed by our rigorous analysis.

We have also reanalyzed the previous polarization measurements of transitions in heliumlike ions [7, 8] in light of our analysis of electron spiraling. The polarization factors for $1s2p\ ^1P_1 \rightarrow 1s^2\ ^1S_1$ ($w$) and $1s2p\ ^3P_2 \rightarrow 1s^2\ ^1S_1$ ($x$) line emission produced by electron impact excitation at threshold are $\gtrsim 0.6$ and $\lesssim -0.5$, respectively. Figure 6 shows the theoretical polarization factors of $w$ and $x$ as a function of atomic number $Z$ for $E_\perp = 0$, 250, and 700 eV. Note that as $Z$ increases, the threshold excitation energy increases, and $E_\perp/E$ decreases. In light of the $1\sigma$ error bars of the measurements, we note again that the effects of electron spiraling is unimportant in these measurements. However, the measured polarization factor of Fe XXV $x$ does strongly suggests that $E_\perp$ was significantly less than 700 eV for the Fe XXIV measurements.

Depolarization of the observed line emission can occur due to electron collision which redistribute the population of the $m$ levels of the excited state. We estimates these effects to be insignificant for the Sc XX, Fe XXIV, and Fe XXV results. If we assume the $m$-changing cross section is $\sim 10^{-16}$ cm$^2$ (a large overestimate

for such highly charged ions), then the $m$-changing rate coefficient is $\sim 3 \times 10^{-7}$ cm$^3$ s$^{-1}$. For typical EBIT electron densities, this yields an $m$-changing rate of $\sim 4 \times 10^5$ s$^{-1}$ which is significantly smaller than the radiative rates for the transitions of interest. However, $m$-changing electron collisions may be important for forbidden transitions with radiative lifetimes of $\sim 1$ $\mu$s.

Polarization measurements have also been carried out for a magnetic quadrupole transition in neonlike barium at energies $\gtrsim 5.0$ keV [9]. The measured polarization ranged between $\sim -0.25$ and 0.05. We expect that electron spiraling probably has an insignificant effect on the measured polarization. The polarization factor is relatively small and the value of $E_\perp/E$ also relatively small.

# 6 Conclusions

We have presented a theoretical formalism for calculating the anisotropy and polarization of photon emission due to a spiraling beam of electrons in an EBIT. We have presented polarization measurements of the Fe XXIV $4p\ ^2P_{3/2} \rightarrow 2s\ ^2S_{1/2}$ transition due to EIE and discussed previously reported measurements in an attempt to determine the importance of electron spiraling. We showed that the effect of electron spiraling is smaller or equal to the accuracy limits of the present measurements. Measurments at very low beam energy, where $E_\perp/E$ approaches unity, may show a strong effect provided statistical uncertainties are kept small. The insensitivity of most crystal spectrometer measurements to spiraling effects is the result of the fact that polarization is in general only a relatively small correction to the observed line intensities. The bulk of this correction can be carried out without knowledge of the exact value of $E_\perp$.

# 7 Acknowledgements

The authors wish to thank K. J. Reed for providing the Fe XXIV electron impact excitation cross sections to magnetic sublevels, D. A. Liedahl for providing the Fe XXIV radiative rates, J. Dubau, V. L. Jacobs, and R. E. Marrs for stimulating conversation, and P. A. D'Antonio, E. W. Magee, and D. H. Nelson for their expert technical support. Work performed at Lawrence Livermore National Laboratory was performed under the auspices of the US Department of Energy (contract W-7405-ENG-48). This program is supported by NASA High Energy Astrophysics X-Ray Astronomy Research and Analysis grant NAG5-5123 (Columbia University) and work order W-19127 (Lawrence Livermore).

# References


[1] I. C. Percival and M. J. Seaton, Phil. Trans. R. Soc. London Ser. A **251**, 113 (1958).

[2] U. Fano and J. H. Macek, Rev. Mod. Phys. **45**, 553 (1973).

[3] M. K. Inal and J. Dubau, J. Phys. B **20**, 4221 (1987).

[4] M. A. Levine, R. E. Marrs, J. R. Henderson, D. A. Knapp, and M. B. Schneider, Phys. Scr. **T22**, 157 (1988).

[5] M. A. Levine, R. E. Marrs, J. N. Bardsley, P. Beiersdorfer, C. L. Bennett, M. H. Chen, T. Cowan, D. Dietrich, J. R. Henderson, D. A. Knapp, A. Osterheld, B. M. Penetrante, M. B. Schneider, and J. H. Scofield, Nucl. Instrum. Methods **B43**, 431 (1989).

[6] R. E. Marrs, in *Experimental Methods in the Physical Sciences, Volume 29A, Atomic Molecular, and Optical Physics: Charged Particles*, eds. F. B. Dunning and R. G. Hulet (Academic Press, San Diego, 1995), 391.

[7] P. Beiersdorfer, D. A. Vogel, K. J. Reed, V. Decaux, J. H. Scofield, K. Widmann, G. Hölzer, E. Förster, O. Wehrhan, D. W. Savin, and L. Schweikhard, Phys. Rev. A **53**, 3974 (1996).

[8] J. R. Henderson, P. Beiersdorfer, C. L. Bennett, S. Chantrenne, D. A. Knapp, R. E. Marrs, M. B. Schneider, K. L. Wong, G. A. Doschek, J. F. Seely, C. M. Brown, R. E. LaVilla, J. Dubau, and M. A. Levine, Phys. Rev. Lett. **65**, 705 (1990)

[9] E. Takács, E. S. Meyer, J. D. Gillaspy, J. R. Roberts, C. T. Chantler, L. T. Hudson, R. D. Deslattes, C. M. Brown, J. M. Lamming, J. Dubau, and M. K. Inal, Phys. Rev. A **54** 1342 (1996)

[10] J. D. Jackson, *Classical Electrodynamics*, (John Wiley & Sons, New York, 1975), 588.

[11] S. Pastuszka, U. Schramm, M. Grieser, C. Broude, R. Grimm, D. Habs, J. Kenntner, H.J. Miesner, T. Schüßler, D. Schwalm, and A. Wolf, Nucl. Instrum. Methods **A369**, 11 (1996).

[12] J. D. Gillaspy, J. R. Roberts, C. M. Brown, and U. Feldman, in *VIth International Conference on the Physics of Highly Charged Ions*, eds. P. Richard, M. Stöckli, C. L. Cocke, and C. D. Lin, AIP Conference Proceedings No. 274 (American Institute of Physics, New York, 1993), 682.

[13] R. M. Steffen and K. Alder, in *The Electromagnetic Interaction in Nuclear Spectroscopy*, ed. W. D. Hamilton (North-Holland Publishing Company, Amsterdam, 1975), 505.

[14] K. Alder and R. M. Steffen, in *The Electromagnetic Interaction in Nuclear Spectroscopy*, ed. W. D. Hamilton (North-Holland Publishing Company, Amsterdam, 1975), 1.

[15] A. Bohr and B. R. Mottelson, *Nuclear Structure: Volume I*, (W. A. Benjamin, Inc., New York, 1969).

[16] R. D. Cowan, *The Theory of Atomic Structure and Spectra*, (University of California, Berkeley, 1981).

[17] A. R. Edmonds, *Angular Momentum in Quantum Mechanics*, (Princeton University Press, Princeton, 1960), pp. 23, 24 & 59.

[18] J. D. Jackson, *Classical Electrodynamics*, (John Wiley & Sons, New York, 1975), 760.

[19] R. E. Marrs, P. Beiersdorfer, S. R. Elliott, D. A. Knapp, and Th. Stoehlker, Phys. Scr. **T59**, 183 (1995).

[20] P. Beiersdorfer, T. W. Phillips, K. L. Wong, R. E. Marrs, and D. A. Vogel, Phys. Rev. A **46**, 3812 (1992).

[21] P. Beiersdorfer, V. Decaux, S. R. Elliot, K. Widmann, and K. Wong, Rev. Sci. Instrum. **66**, 303 (1995).

[22] P. Beiersdorfer, V. Decaux, and K. Widmann, Nucl. Instrum. Methods **B98**, 566 (1995).

[23] P. Beiersdorfer and B. J. Wargelin, Rev. Sci. Instrum. **65**, 13 (1994).

[24] P. Beiersdorfer, J. R. Crespo López-Urrutia, E. Förster, J. Mahiri, and K. Widmann, Rev. Sci. Instrum. **68**, 1077 (1997).

[25] A. H. Compton and S. K. Allison, *X-Rays in Theory and Experiment*, (D. Van Nostrand Company, Inc., New York, 1935), Chapter VI.

[26] B. L. Henke, E. M. Gullikson, and J. C. Davis, At. Data Nucl. Data Tables, **54**, 181 (1993).

[27] C. J. Borkowski and M. K. Kopp, Rev. Sci. Instrum. **39**, 1515 (1968).

[28] B. J. Wargelin, P. Beiersdorfer, D. A. Liedahl, S. M. Kahn, and S. von Goeler, Astrophys. J. (accepted).

[29] D. W. Savin, P. Beiersdorfer, J. Crespo López-Urrutia, V. Decaux, E. M. Gullikson, S. M. Kahn, D. A. Liedahl, K. J. Reed, and K. Widmann, Astrophys. J. **470**, L73 (1996).

[30] P. R. Bevington, *Data Reduction and Error Analysis for the Physical Sciences*, (McGraw-Hill, New York, 1969), 64.

[31] Ö Adell, G. Brogren, and L.-E. Haeggblom, Ark. Fys. **7**, 197 (1953).

[32] M. A. Blokhin, *X-Ray Spectroscopy*, (Hindustan Publishing Corporation, Delhi, 1962), 231.

[33] N. G. Alexandropoulos and G. C. Cohen, Appl. Spectrosc. **28**, 155 (1974).

[34] D. M. Barrus, R. L. Blake, H. Felthauser, E. E. Fenimore, and A. J. Burek, in *Low Energy X-ray Diagnostics–1981*, ed. D. T. Attwood and B. L. Henke, AIP Conference Proceedings No. 75, (American Institute of Physics: New York, 1981), 115.

[35] G. Brogren, Ark. Fys. **22**, 267 (1962).

[36] R. L. Kelly, J. Phys. Chem. Ref. Data **16**, Suppl. 1 (1987).

[37] H. L. Zhang, D. H. Sampson, and R. E. H. Clark, Phys. Rev. A **41**, 198 (1990).

[38] M. Klapisch, J. L. Schwob, B. S. Fraenkel, and J. Oreg, J. Opt. Soc. Am. **67**, 148 (1977).